Manufacturing Letters 28 (2021) 25–29

Contents lists available at ScienceDirect

Manufacturing Letters

journal homepage: www.elsevier.com/locate/mfglet

Letters

Effect of temperature history on thermal properties of additively manufactured C-18150 alloy samples

Congyuan Zeng [a], Hao Wen [a], Benjamin C. Bernard [b], Jonathan R. Raush [b], Paul R. Gradl [c], Michael Khonsari [a], S.M. Guo [a,*]

[a] Dept. Mechanical & Industrial Engineering, Louisiana State University, Baton Rouge, LA 70803, USA
[b] Dept. Mechanical Engineering, University of Louisiana at Lafayette, Lafayette, LA 70503, USA
[c] NASA/Marshall Space Flight Center, Huntsville, AL 35812, USA

ARTICLE INFO

Article history:
Received 25 November 2020
Received in revised form 4 February 2021
Accepted 18 February 2021
Available online 11 March 2021

Keywords:
C-18150 alloy
Thermal property
Additive manufacturing
Heat treatment

ABSTRACT

The effects of thermal history on the thermal properties of C-18150 (Cu-1.5Cr-0.5Zr, wt%) parts made by the laser powder-bed-fusion (L-PBF) additive manufacturing (AM) process with three different fabrication orientations (horizontal, angled, and vertical to the build direction) were investigated. A significant difference in thermal properties between as-fabricated and fully heat-treated L-PBF C-18150 samples was observed, and the mechanisms of such behaviors are discussed.

1. Introduction

NASA and their aerospace industry partners are exploring the Laser Powder-Bed-Fusion (L-PBF) additive manufacturing (AM) process for building liquid rocket engine components with copper alloys [1,2]. Due to the extremely fast cooling rate of the L-PBF process (10^6–10^7 K/s [3]), non-equilibrium states, i.e. supersaturated solid-solutions [4], typically exist, leading to unique thermal, electrical, and mechanical properties for the as-fabricated L-PBF components.

Copper alloy C-18150 is a precipitation-hardened CuCrZr alloy. The effects of heat treatment on CuCrZr alloys prepared by conventional fabrication methods [5–13] and recently by the L-PBF method [14] were investigated. Most of those studies focused on the mechanical and electrical properties. For thermal properties, Hanzelka et al. [15] studied the low-temperature thermal conductivity of Cu-0.71Cr-0.23Zr alloy form 5 K to 300 K, and Krishna et al. [16] performed investigations on thermal conductivity of Cu-0.61Cr-0.038Zr-0.029Ti alloy from 300 K to 873 K. Over the testing temperature, both studies found that thermal conductivity increased with the rise of testing temperature. However, very limited research was conducted on the high-temperature thermal performance of CuCrZr parts made by AM, which is a critical property for liquid rocket engine components. For this reason, this study focuses on the high-temperature thermal properties of L-PBF C-18150 samples. A significant difference in thermal properties between as-fabricated and fully heat-treated L-PBF C-18150 samples was observed, and the mechanisms of such behaviors are discussed.

2. Materials and methods

Cylindrical-shaped L-PBF C-18150 samples were fabricated in three different orientations: vertical, angled (45°), and horizontal to the build direction. The schematics indicating the orientations of the samples are shown in Fig. 1a. Hereafter, the samples are denoted as Vertical, Angled, and Horizontal, respectively. Thermal properties of the C-18150 AM samples were evaluated using a Netzsch LFA 467 apparatus from room temperature (RT) to 1000 C at a heating rate of 25 °C/min, with a dwell time of ~30 min at each testing temperature (except RT). The detailed description of the testing process can be found elsewhere [17]. X-ray diffraction (XRD) was utilized to characterize the phase structures, with the tested surfaces perpendicular to the central axis of the sample cylinders.

* Corresponding author.
E-mail address: sguo2@lsu.edu (S.M. Guo).

https://doi.org/10.1016/j.mfglet.2021.02.002

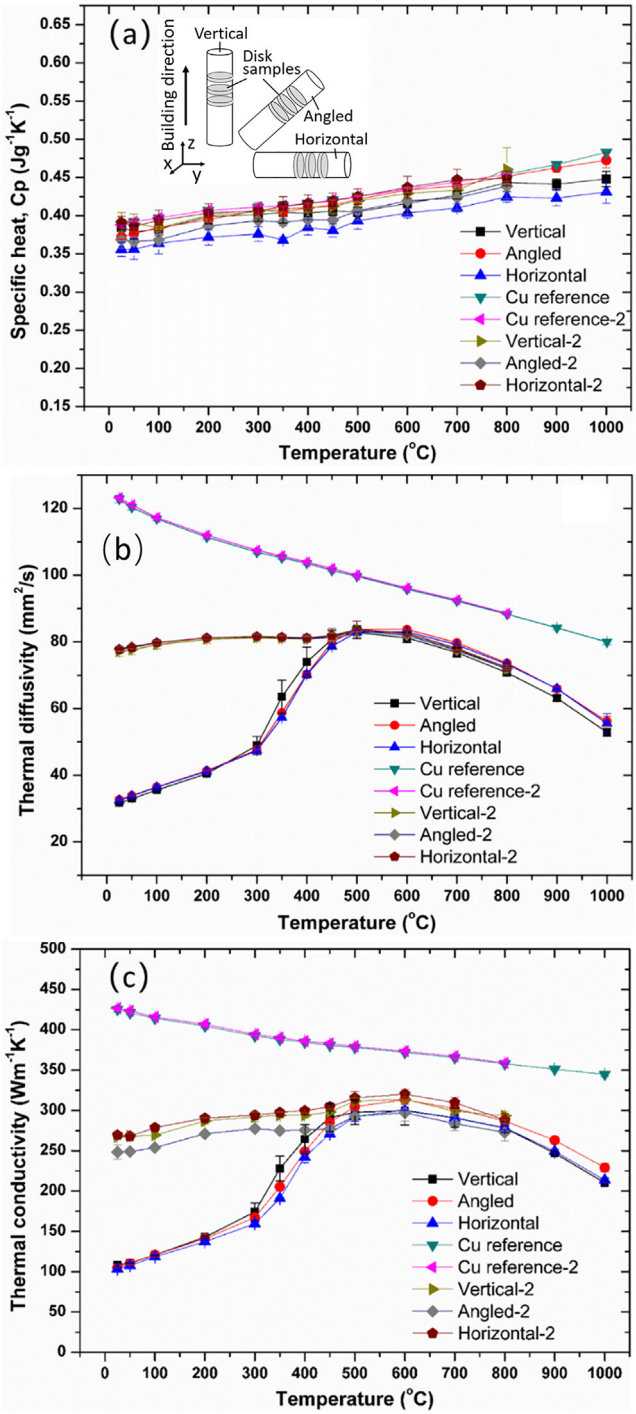

Fig. 1. Thermal properties of the as-fabricated samples with vertical, angled, and horizontal fabrication orientations, together with a pure copper reference sample of the first and the second test cycle. (a), (b) and (c) show the variation of specific heat, thermal diffusivity and thermal conductivity as a function of testing temperature, respectively. "-2" indicates the repeated test cycle.

3 . Results and discussion

3.1. Thermal property test

The Netzsch LFA 467 measures thermal diffusivity directly and provides specific heat measurements by comparing the samples with a pure Cu reference sample. Thermal conductivity is the product of thermal diffusivity, specific heat, and density. Densities of the L-PBF C-18150 samples were measured using the Archimedes principle, and the densities of Horizontal, Angled, and Vertical samples were 8.94 ± 0.08, 8.63 ± 0.08, 8.87 ± 0.13 g/cm^3, respectively. In the first test cycle, thermal diffusivity/conductivity values for the as-fabricated samples were unexpectedly low from RT to ~500 C, Fig. 1. This motivated the authors to repeat the test with a second cycle. The specific heat values of L-PBF C-18150 samples (Fig. 1a) were found to increase monotonically from RT to 1000 C and no clear differences were observed among all the samples over the two test cycles, indicating that specific heat is non-sensitive to the thermal history.

Based on Fig. 1b and c, thermal diffusivity was clearly the decisive factor influencing thermal conductivity measurements. Meanwhile, samples with different fabrication orientations had almost identical thermal diffusivity/conductivity values, indicating that thermal diffusivity and conductivity are not sensitive to grain orientation, which agrees with a previous study [18]. During the first test cycle, thermal diffusivity increased from RT to around 500 C, and then declined while progressing to temperatures up to 1000 C. Due to the heat-treatment effect of the first test cycle, thermal diffusivity of the second cycle was clearly higher than that of the first cycle when tested below 500 C. However, above 500 C, the thermal diffusivity measurements of the two cycles overlapped.

3.2. Mechanisms behind the variations of thermal properties for the as-fabricated C-18150 samples

C-18150 is a precipitate-strengthened alloy with dilute Cr/Zr elements. As heat is mainly carried by electrons in metals [19], a small addition of solute atoms would dramatically increase electrical resistivity and remarkably reduce thermal conductivity [20–23]. The authors performed CALPHAD calculations (ThermoCalc software package, TCCU3 database) to highlight the solidification process and the formation of precipitates at different temperatures (Fig. 2) [24]. CALPHAD calculation predicts the phase equilibrium at different temperatures using the Gibbs energy principle [25]. Based on CALPHAD calculations, the amount of phases in C-18150 at equilibrium state over a wide temperature range is plotted, i.e. Fig. 2. Obviously, in an equilibrium condition, the dominant phase of C-18150 alloy at RT is the Cu phase (FCC_L12). The precipitates in C-18150 include Cr (BCC_B2), $Cu_{51}Zr_{14}$, and Cr_2Zr (C15_LAVES). And the total amount of secondary phases is <2% (Fig. 2b). At 630 °C, $Cu_{51}Zr_{14}$ transforms into Cu_2Zr. Due to the rapid cooling process associated with AM, the as-fabricated C-18150 samples have supersaturated Cr/Zr solute atoms in the Cu matrix, which significantly scatter electrons [26–29], thus resulting in a low thermal conductivity. With the increase of testing temperature, solute Cr/Zr atoms gradually form precipitates, reducing thermal resistance. At low testing temperatures (<500 C), solute atoms act as the decisive scattering center for free electrons, and the decrease of solute atoms reduces thermal resistance and consequently increases thermal diffusivity/conductivity. However, at high temperatures, electron–phonon interactions become stronger [30] and the thermal diffusivity/conductivity of C-18150 L-PBF alloy therefore decreases monotonically with an increase in testing temperatures over 500 C (Fig. 1b, c).

3.3. Effect of temperature history on thermal properties of C-18150 AM samples

The precipitation process depends on the aging temperature [14,31]. To examine the effect of temperature history on the precipitation process of L-PBF C-18150 samples, heat treatments were performed on as-fabricated Vertical samples at 420, 500, 575, and 650 C, each for 2 h.

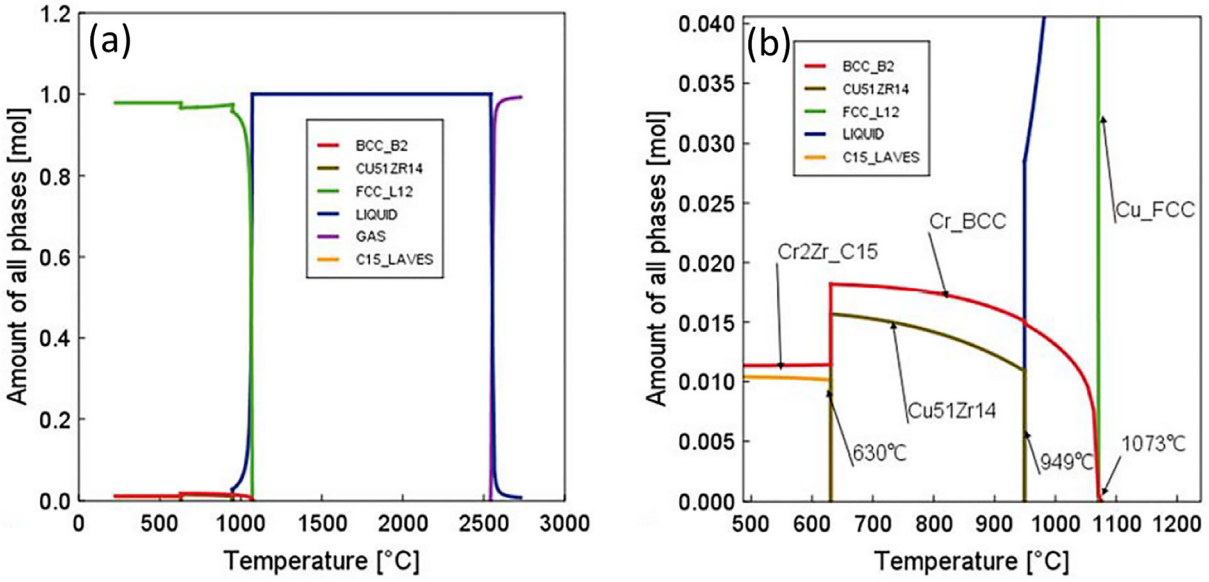

Fig. 2. CALPHAD study of C-18150 alloy. (a) Full range calculation results, (b) minor phases.

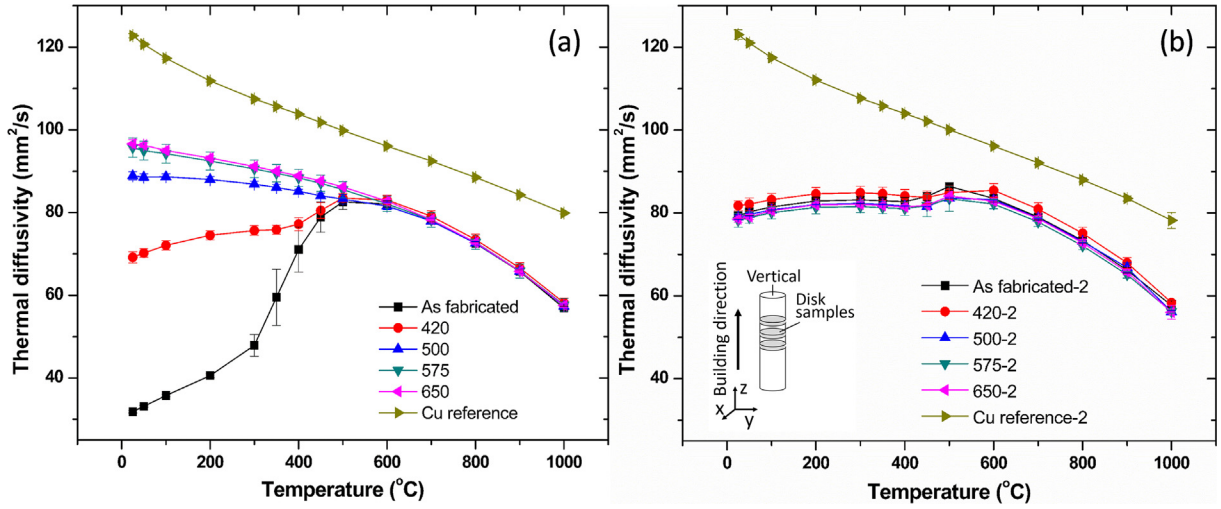

Fig. 3. Images showing the thermal diffusivity results of the aged Vertical samples after the first test cycle (a) and the second test cycle (b).

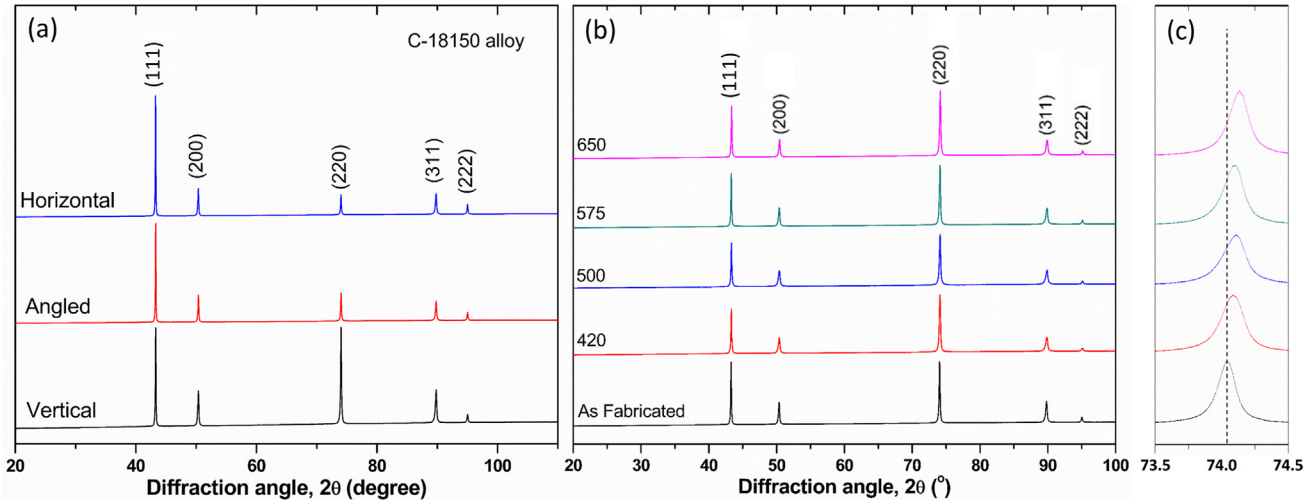

Fig. 4. Images showing XRD results of the as-fabricated samples and aged Vertical samples. (a) As-fabricated samples with different fabrication orientations. (b) Samples aged at different temperatures. (c) Shift of diffraction peaks at varying aging temperatures.

Thermal diffusivity results for the two test cycles are shown in Fig. 3. Clearly, when tested below 500 C during the first cycle, thermal diffusivity of the samples increased relative to the aging temperature (Fig. 3a) due to the enhanced precipitation. Thermal diffusivity of the samples converged above 500 C, at which point nearly all the solute Cr/Zr atoms had formed precipitates and the phonon-electron interaction dominated. Samples aged at high temperatures (575 and 650 C) showed nearly identical thermal diffusivity, indicating aging at 575 C for 2 h was sufficient to complete the precipitation process. Thermal diffusivity of the second test cycle was almost identical for all the samples (Fig. 3b). It is noteworthy that at low testing temperatures (<400 C), thermal diffusivity of the second test cycle (for samples aged above 500 C) was lower than that of the first test cycle, which is most likely caused by the over-aging effect during the first cycle, introducing non-coherency between the precipitates and Cu matrix [18,20], and causing higher thermal resistance. With an aging temperature over 500 C for 2 h, an improved thermal conductivity of ~280 W/(m·K) at RT was obtained.

Consistent with the CALPHAD study, XRD results showed that, for both the as-fabricated and aged samples, the dominant phase is FCC-Cu (Fig. 4a, b). For the as-fabricated samples, the Cu(220) peak became stronger when the fabrication orientation changed from horizontal to vertical, indicating preferential grain growth (Fig. 4a). For the aged samples, the diffraction peaks shifted towards larger diffraction angles as aging temperature increased (Fig. 4c), which, per Bragg's equation [13], indicates a decrease of lattice parameter caused by the gradual precipitation of solute Cr/Zr atoms [14]. This verifies the variation behaviors of thermal properties observed in Fig. 3.

4. Conclusions

C-18150 L-PBF samples were characterized to investigate the effect of temperature history on the thermal properties. The following conclusions are reached.

(1) FCC-Cu is the dominant phase of the C-18150 alloy. Due to the extremely rapid cooling rate of the L-PBF process, Cr/Zr atoms are supersaturated in the Cu matrix.
(2) Specific heat is not sensitive to the thermal history, while thermal diffusivity is not sensitive to grain orientation.
(3) Thermal diffusivity is the dominant factor influencing thermal conductivity. Due to the supersaturated solid solutes, the as-fabricated L-PBF C-18150 samples have much reduced thermal conductivity values at RT to about 500 °C. However, heat treatment above 500 °C for 2 h can effectively recover the thermal properties of the L-PBF C-18150 alloy due to the precipitation of Cr/Zr solid solute atoms.

Declaration of Competing Interest

The authors declare that they have no known competing financial interests or personal relationships that could have appeared to influence the work reported in this paper.

Acknowledgements

This work is supported by the National Aeronautics and Space Administration (NASA)'s Established Program to Stimulate Competitive Research (EPSCoR) Cooperative Agreement number 80NSSC19M0079 (CFDA number 43.008). The use of instruments housed within the LSU Shared Instrumentation Facilities (SIF), a part of LAMDA (grant number NSF #OIA-1946231) Core User Facilities, is acknowledged. The C-18150 L-PBF samples were produced by Moog (www.moog.com).

References

[1] Gradl PR, Protz C, Greene SE, Ellis D, Lerch B, Locci I. Development and hot-fire testing of additively manufactured copper combustion chambers for liquid rocket engine applications. 53rd AIAA/SAE/ASEE Joint Propulsion Conference 2017:4670. https://doi.org/10.2514/6.2017-4670.
[2] Gradl PR, Protz CS, Ellis DL, Greene SE, Progress in Additively Manufactured Copper-Alloy GRCop-84, GRCop-42, and Bimetallic Combustion Chambers for Liquid Rocket Engines 2019.
[3] Hooper PA. Melt pool temperature and cooling rates in laser powder bed fusion. Addit Manuf 2018;22:548–59. https://doi.org/10.1016/j.addma.2018.05.032.
[4] Knoop D, Lutz A, Mais B, von Hehl A. A tailored AlSiMg alloy for laser powder bed fusion. Metals 2020;10(4):514. https://doi.org/10.3390/met10040514.
[5] Holzwarth U, Stamm H, Pisoni M, Volcan A, Scholz R. The recovery of tensile properties of CuCrZr alloy after hot isostatic pressing. Fusion Eng Des 2000;51:111–6. https://doi.org/10.1016/S0920-3796(00)00384-7.
[6] Barabash V, Kalinin G, Fabritsiev SA, Zinkle SJ. Specification of CuCrZr alloy properties after various thermo-mechanical treatments and design allowables including neutron irradiation effects. J Nucl Mater 2011;417(1–3):904–7. https://doi.org/10.1016/j.jnucmat.2010.12.158.
[7] Park J-Y, Jung Y-I, Choi B-K, Lee J-S, Jeong YH, Hong BG. Investigation on the microstructure and mechanical properties of CuCrZr after manufacturing thermal cycle for plasma facing component. J Nucl Mater 2011;417(1–3):916–9. https://doi.org/10.1016/j.jnucmat.2010.12.157.
[8] Merola M, Orsini A, Visca E, Libera S, Moreschi LF, Storai S, et al. Influence of the manufacturing heat cycles on the CuCrZr properties. J Nucl Mater 2002;307-311:677–80. https://doi.org/10.1016/S0022-3115(02)01186-8.
[9] Ivanov A, Nikolaev A, Kalinin G, Rodin M. Effect of heat treatments on the properties of CuCrZr alloys. J Nucl Mater 2002;307:673–6. https://doi.org/10.1016/S0022-3115(02)01110-8.
[10] Edwards D, Singh BN, Tähtinen S. Effect of heat treatments on precipitate microstructure and mechanical properties of a CuCrZr alloy. J Nucl Mater 2007;367:904–9. https://doi.org/10.1016/j.jnucmat.2007.03.064.
[11] Park J-Y, Lee J-S, Choi B-K, Hong BG, Jeong YH. Effect of cooling rate on mechanical properties of aged ITER-grade CuCrZr. Fusion Eng Des 2008;83(10–12):1503–7. https://doi.org/10.1016/j.fusengdes.2008.07.006.
[12] Gillia O, Briottet L, Chu I, Lemoine P, Rigal E, Peacock A. Characterization of CuCrZr and CuCrZr/SS joint strength for different blanket components manufacturing conditions. J Nucl Mater 2009;386:830–3. https://doi.org/10.1016/j.jnucmat.2008.12.244.
[13] Kalinin G, Ivanov A, Obushev A, Rodchenkov B, Rodin M, Strebkov Y. Ageing effect on the properties of CuCrZr alloy used for the ITER HHF components. J Nucl Mater 2007;367:920–4. https://doi.org/10.1016/j.jnucmat.2007.03.256.
[14] Wallis C, Buchmayr B. Effect of heat treatments on microstructure and properties of CuCrZr produced by laser-powder bed fusion. Mater Sci Eng A 2019;744:215–23. https://doi.org/10.1016/j.msea.2018.12.017.
[15] Hanzelka P, Musilova V, Kralik T, Vonka J. Thermal conductivity of a CuCrZr alloy from 5 K to room temperatures. Cryo 2010;50(11–12):737–42. https://doi.org/10.1016/j.cryogenics.2010.08.001.
[16] Krishna SC, Supriya N, Jha AK, Pant B, Sharma S, George KM. Thermal conductivity of Cu-Cr-Zr-Ti alloy in the temperature range of 300–873 K. Int Sch Res Notices 2012;2012. https://doi.org/10.5402/2012/580659.
[17] Zeng C, Zhang B, Hemmasian Ettefagh A, Wen H, Yao H, Meng WJ, et al. Mechanical, thermal, and corrosion properties of Cu-10Sn alloy prepared by laser-powder-bed-fusion additive manufacturing. Addit Manuf 2020;35:. https://doi.org/10.1016/j.addma.2020.101411101411.
[18] Olafsson P, Sandstrom R, Karlsson Å. Comparison of experimental, calculated and observed values for electrical and thermal conductivity of aluminium alloys. J Mater Sci 1997;32(16):4383–90. https://doi.org/10.1023/A:1018680024876.
[19] Zhang Y, Stocks GM, Jin K, Lu C, Bei H, Sales BC, et al. Influence of chemical disorder on energy dissipation and defect evolution in concentrated solid solution alloys. Nat Commun 2015;6(1):1–9. https://doi.org/10.1038/ncomms9736.
[20] Su C, Li D, Luo AA, Ying T, Zeng X. Effect of solute atoms and second phases on the thermal conductivity of Mg-RE alloys: A quantitative study. J Alloy Compd 2018;747:431–7. https://doi.org/10.1016/j.jallcom.2018.03.070.
[21] Rudajevova A, Staněk M, Lukáč P. Determination of thermal diffusivity and thermal conductivity of Mg–Al alloys. Mater Sci Eng, A 2003;341(1–2):152–7. https://doi.org/10.1016/S0921-5093(02)00233-2.
[22] Shijie Z, Bingjun Z, Zhen Z, Xin J. Application of lanthanum in high strength and high conductivity copper alloys. J Rare Earths 2006;24(1):385–8. https://doi.org/10.1016/S1002-0721(07)60408-6.
[23] Han SZ, Gu JH, Lee JH, Que ZP, Shin JH, Lim SH, et al. Effect of V addition on hardness and electrical conductivity in Cu-Ni-Si alloys. Met Mater Int 2013;19(4):637–41. https://doi.org/10.1007/s12540-013-4002-x.
[24] Andersson J, Helander T, Höglund L, Shi P, Sundman B. Calphad-based Thermocalc and Dictra method. Calphad 2002;26:273–312.
[25] Andersson J-O, Helander T, Höglund L, Shi P, Sundman B. Thermo-Calc & DICTRA, computational tools for materials science. Calphad 2002;26(2):273–312. https://doi.org/10.1016/S0364-5916(02)00037-8.

[26] Sağlam I, Özyürek D, Çetinkaya K. Effect of ageing treatment on wear properties and electrical conductivity of Cu-Cr-Zr alloy. Bull Mater Sci 2011;34(7):1465–70.
[27] Zhang S, Li R, Kang H, Chen Z, Wang W, Zou C, et al. A high strength and high electrical conductivity Cu-Cr-Zr alloy fabricated by cryorolling and intermediate aging treatment. Mater Sci Eng, A 2017;680:108–14. https://doi.org/10.1016/j.msea.2016.10.087.
[28] Sun L, Tao N, Lu K. A high strength and high electrical conductivity bulk CuCrZr alloy with nanotwins. Scr Mater 2015;99:73–6. https://doi.org/10.1016/j.scriptamat.2014.11.032.
[29] Lin G, Wang Z, Zhang M, Zhang H, Zhao M. Heat treatment method for making high strength and conductivity Cu–Cr–Zr alloy. Mater Sci Technol 2011;27(5):966–9. https://doi.org/10.1179/026708310X12815992418210.
[30] Tritt TM. Thermal conductivity: theory, properties, and applications, Springer Science & Business Media 2005.
[31] Gray V, Galvin D, Sun L, Gilbert E, Martin T, Hill P, et al. Precipitation in a novel maraging steel F1E: A study of austenitization and aging using small angle neutron scattering. Mater Charact 2017;129:270–81. https://doi.org/10.1016/j.matchar.2017.05.002.